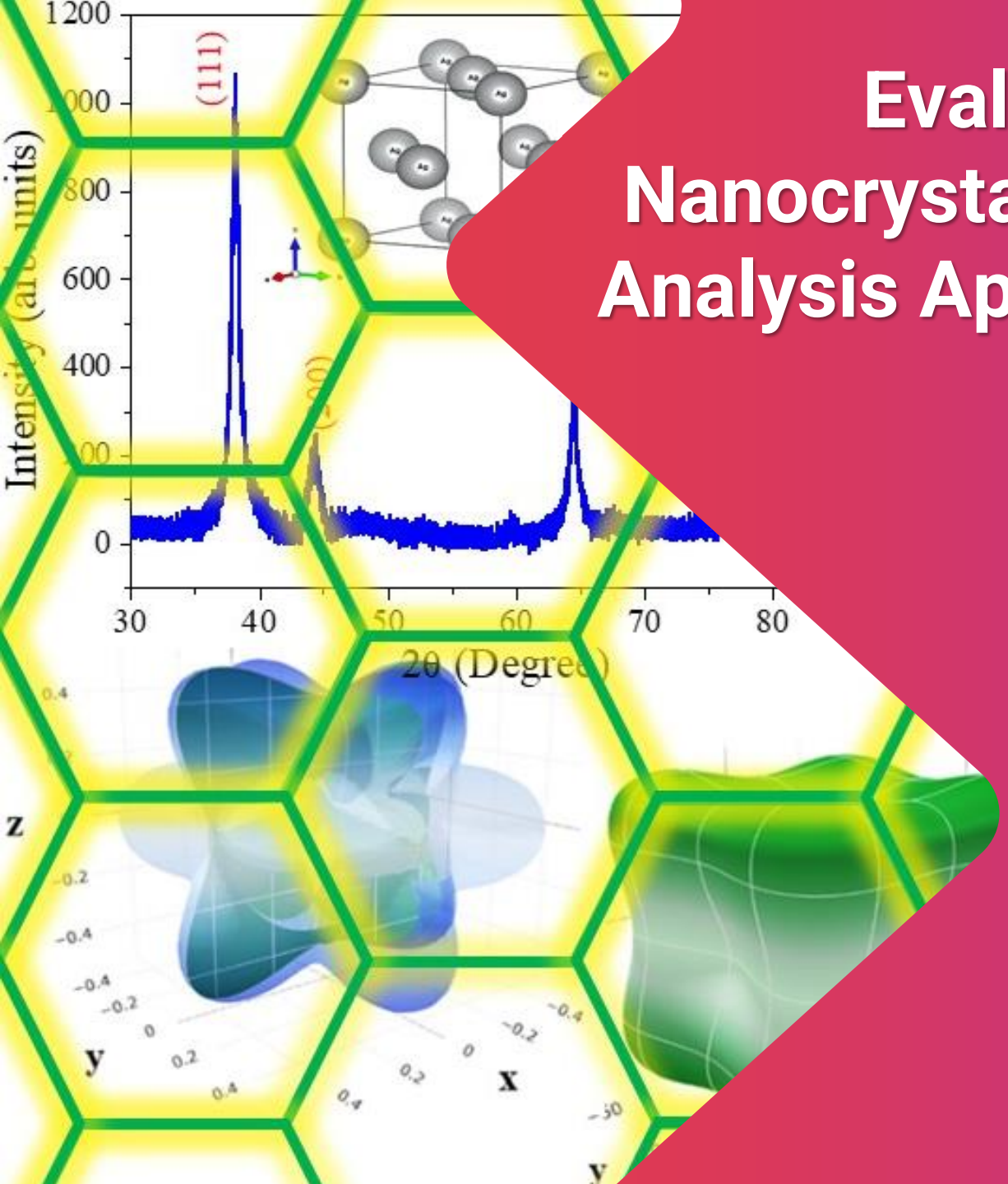


Evaluation of Elastic Properties of Nanocrystalline Silver Using a Combined Analysis Approach: X-Ray Diffraction and Density Functional Theory

Dr. Rahul Das

Assistant Professor
Department of Physics
The University of Burdwan,
Burdwan – 713 104

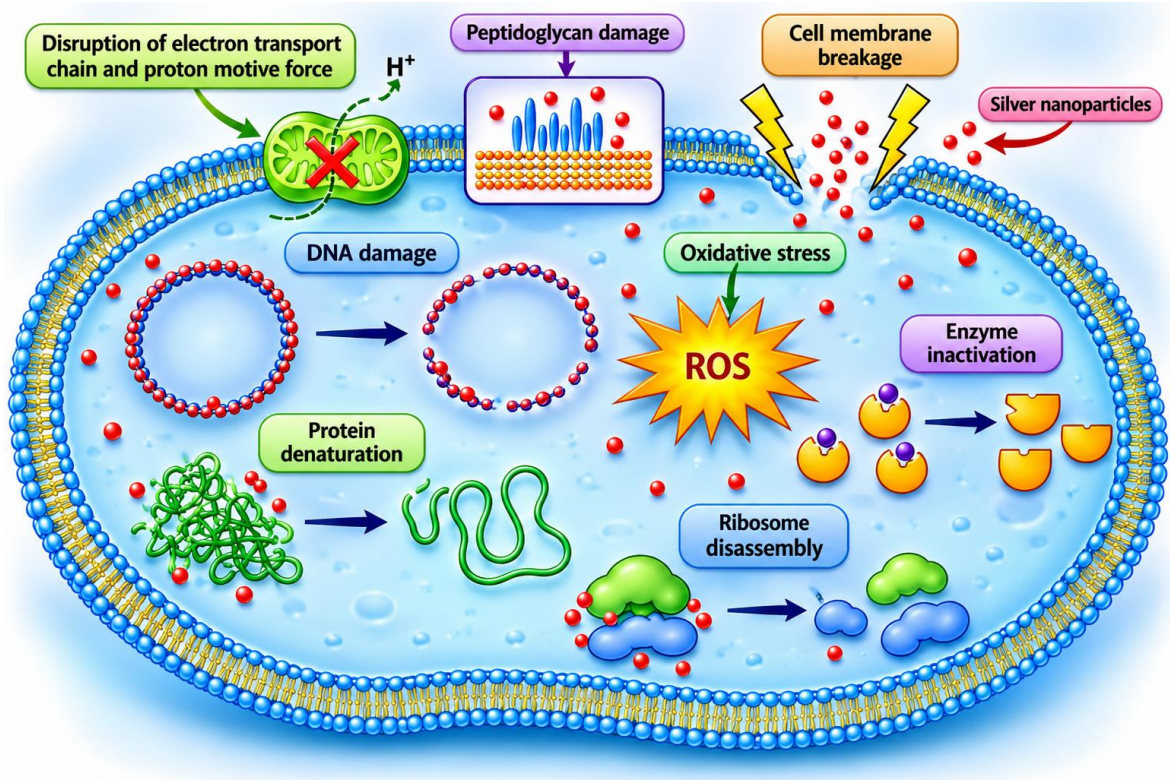
PANE 2026

Nano Silver and its specialities

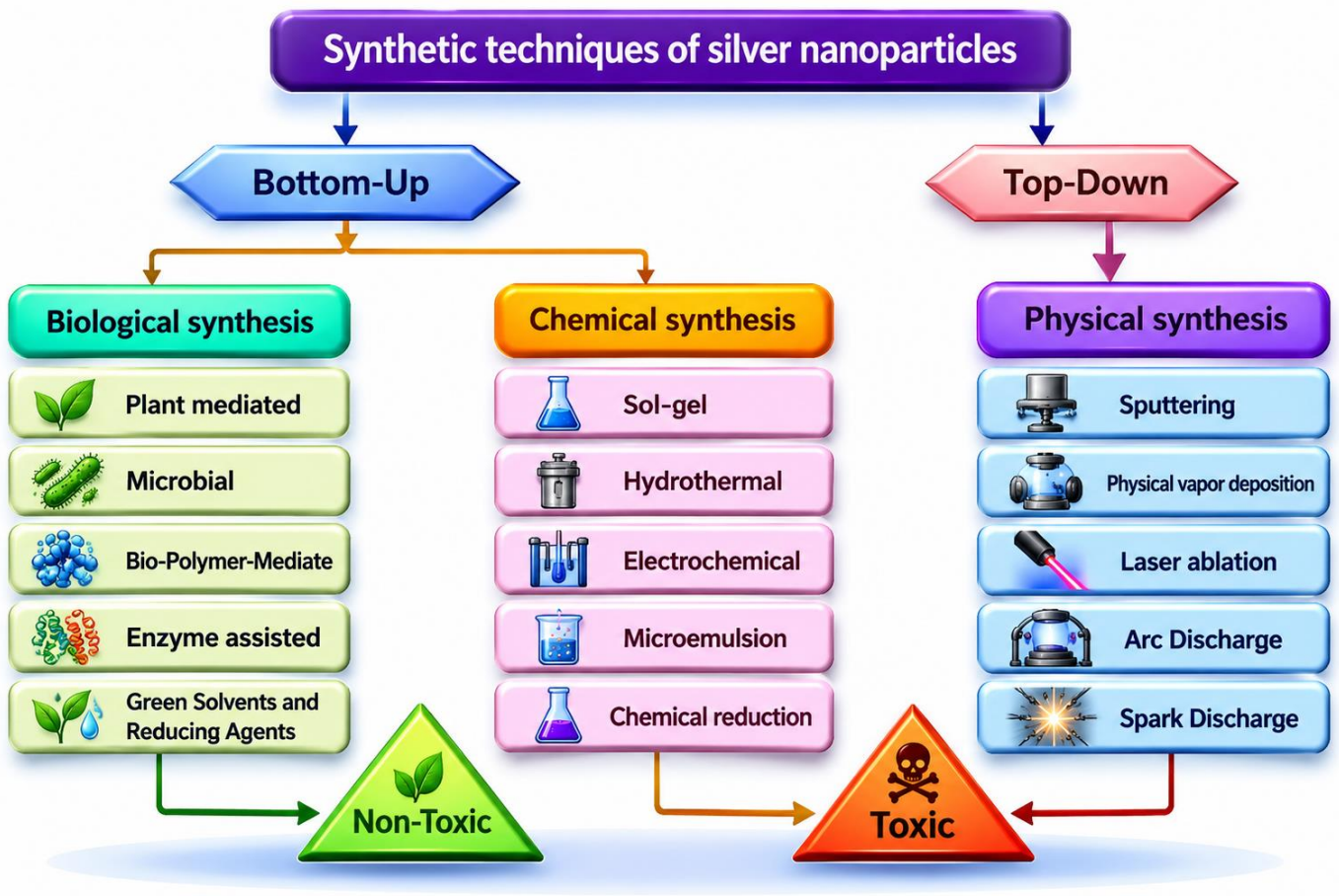
- Nano silver has particles that ranges between 1 to 100 nanometres in size unlocks a massive surface-area-to-volume ratio and emergent physical properties that bulk silver does not possess
- These small particles (nano size particles) are made up of only a few hundred atoms (atom size =>0.1 nm).



- Possible morphologies of nano size particles (nanoparticles) are conical, cubes, polyhedrons, rods, monopods, rings, etc.
- These tiny powders can be used in various application fields such as electronic devices, drug delivery, nano-fertilizers, antimicrobial, anti-cancer, photocatalytic, etc.

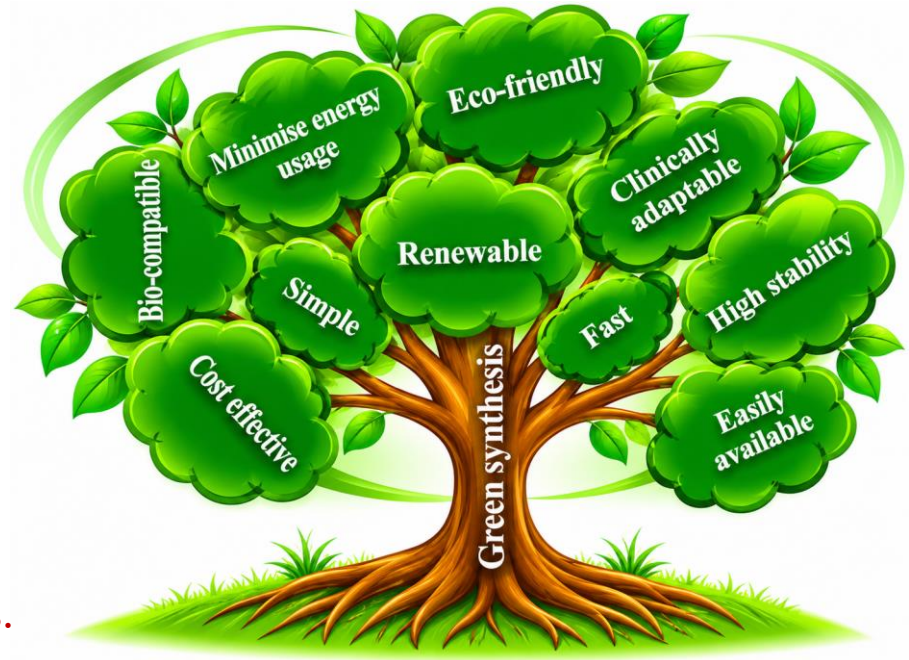


Synthesis Methods of Nanocrystalline Silver



Plant-based Synthesis

- The **plant-mediated method** belongs to the **bottom-up** approach, similar to the **co-precipitation** method.
- This process only uses plant extracts with the metallic precursors to fabricate the desired nanopowders.
- Here plant biomolecules/phytochemicals present in the extracts act as reducing, capping, and stabilizing agents.
- Plant biomolecules are valuable alternative to harmful and expensive chemicals.



- **Top-down approach:** breaking down bulk materials into required nanostructures.
- **Bottom-up approach:** Assembling single atoms and molecules into nanostructures.

Synthesis of AgNPs using *Ocimum tenuiflorum* bud extract

1. Collection & Washing



Ocimum tenuiflorum buds cluster (with green stem)



Wash several times with tap water and then with double distilled water

2. Preparation of Plant Extract



10 g washed buds crushed in mortar and pestle



Add 100 ml DD water



Boil for 10 min at 80 °C

3. Filtration & Centrifugation



Cool and filter with Whatman filter paper



Centrifuge for 20 min at 2000 rpm



Collect supernatant (plant extract)

4. Synthesis of Silver Nanoparticles (AgNPs)



45 mL 1 mM $AgNO_3$ solution



Add 5 mL plant extract gradually



Heat at 80 °C for 15 min with magnetic stirrer



Colour change: Light yellow → Brown (indicates AgNPs formation)

5. Separation of AgNPs



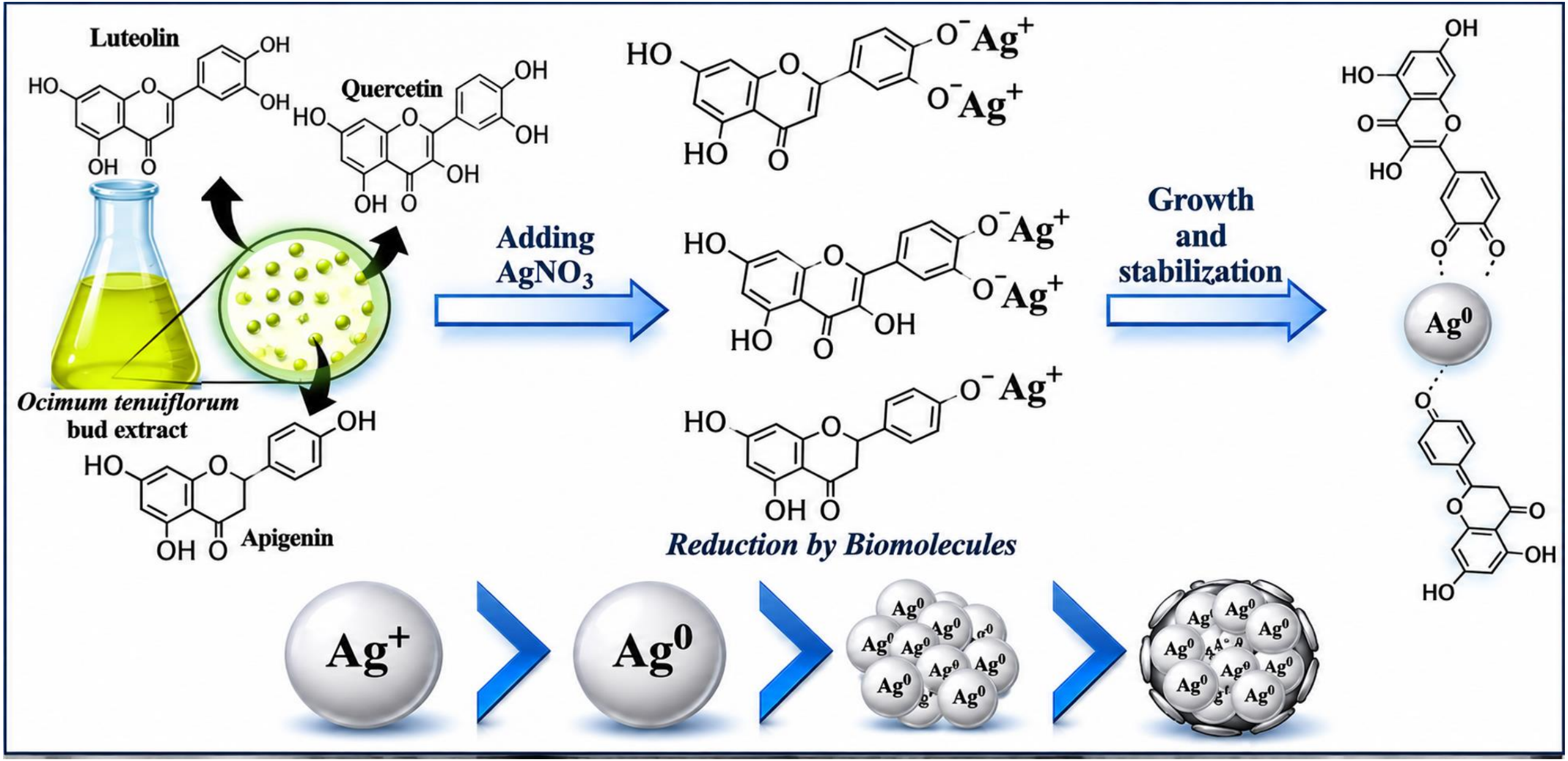
Centrifugation to separate AgNPs



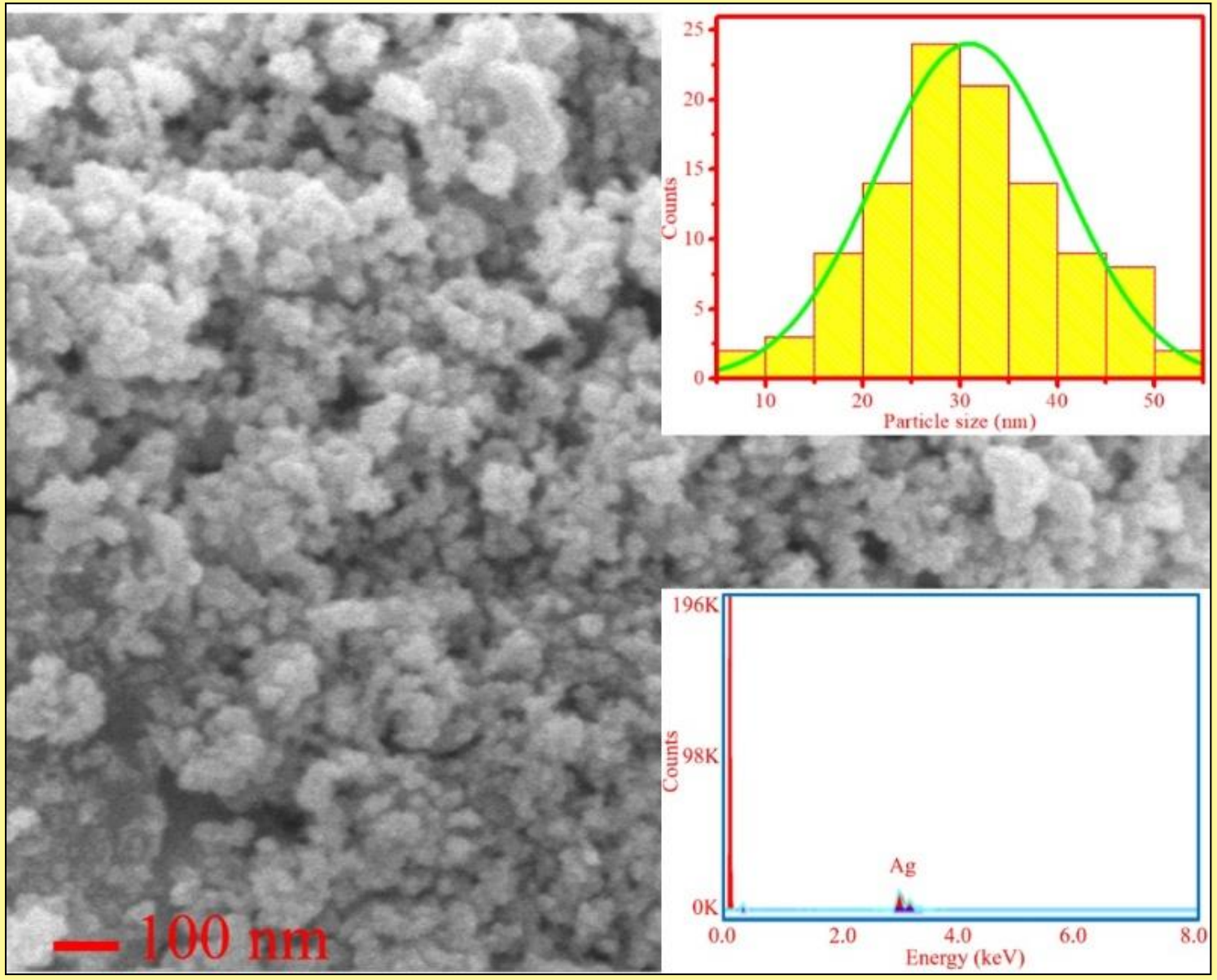
AgNPs

Green Synthesis of Silver Nanoparticles (AgNPs) Using *Ocimum tenuiflorum* Bud Extract

Possible Formation Mechanism of AgNPs



FESEM micrograph and EDX spectrum



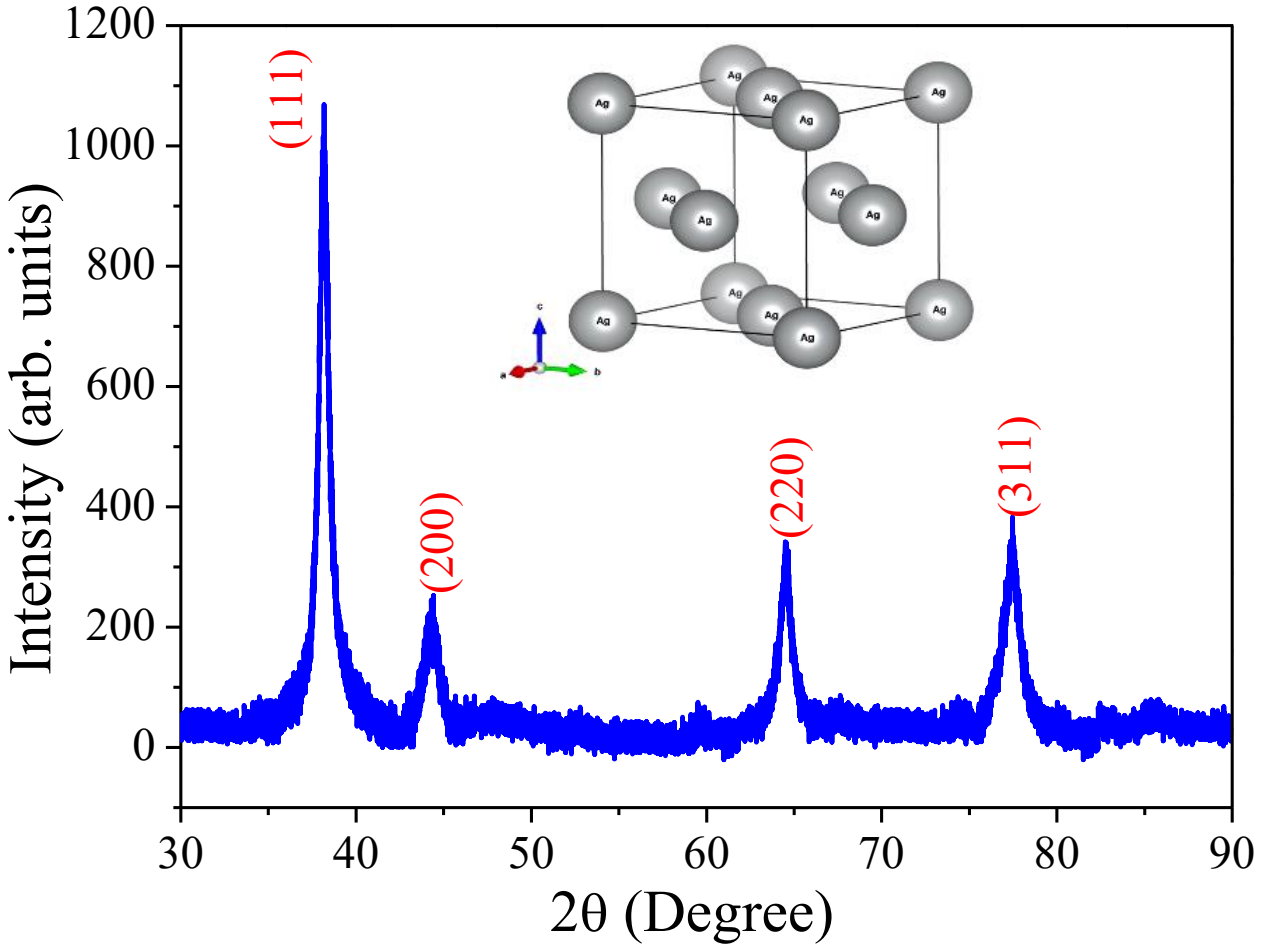
FESEM micrograph reveals that the synthesized Ag particles predominantly exhibit a quasi-spherical morphology. The particle-size distribution histogram indicates a diameter ranging from approximately 5 to 55 nm, with an average particle diameter of around 30 nm.

The EDX spectrum exhibits characteristic signals associated with elemental Ag, confirming that silver is the predominant constituent of the synthesized nanopowder.

These morphological and compositional observations provide an initial assessment of the synthesized material and establish the basis for its subsequent crystallographic and elastic-property investigations.

XRD-Based Structural Analysis

Four prominent diffraction maxima are observed at approximately 38.2°, 44.3°, 64.5°, and 77.4°, corresponding to the (111), (200), (220), and (311) crystallographic planes, respectively. The observed diffraction positions are in good agreement with the standard reference data for metallic silver (JCPDS Card No. 00-004-0783), confirming the formation of a face-centred cubic (FCC) crystalline phase belonging to the Fm-3m space group (No. 225).



$$2d_{hkl}Sin\,\theta = n\lambda$$

$$\text{and } a = d_{hkl}\sqrt{h^2 + k^2 + l^2}$$

$$V_{uc} = a^3$$

$$r_{Ag} = a/2\sqrt{2}$$

$$APF = \left[\frac{Z\left(\frac{4}{3}\pi r_{Ag}^3\right)}{V_{uc}}\right] \text{ and } \rho = ZM_w/N_A V_{uc}$$

(hkl) Plane	2θ(°)	d_{hkl} (nm)	a (nm)	mean a (nm)	V_{cu} (nm^3)	r_{Ag} (nm)	APF	P (g/cm^3)
(111)	38.2	0.2356	0.409	0.408	0.068	0.14	0.74	10.52
(200)	44.3	0.2043	0.408					
(220)	64.5	0.1444	0.408					
(311)	77.4	0.1232	0.408					

Crystallite Size and Lattice Microstrain Analysis

The broadening of XRD diffraction peaks is primarily associated with the finite dimensions of coherently diffracting crystalline domains and lattice microstrain arising from crystal imperfections, defects, and local lattice distortions.

The corrected broadening

$$\beta_c^2 = \beta_{obs}^2 - \beta_{ins}^2$$

Scherrer equation

$$D_{hkl} = k\lambda/\beta_{hkl} Cos\,\theta$$

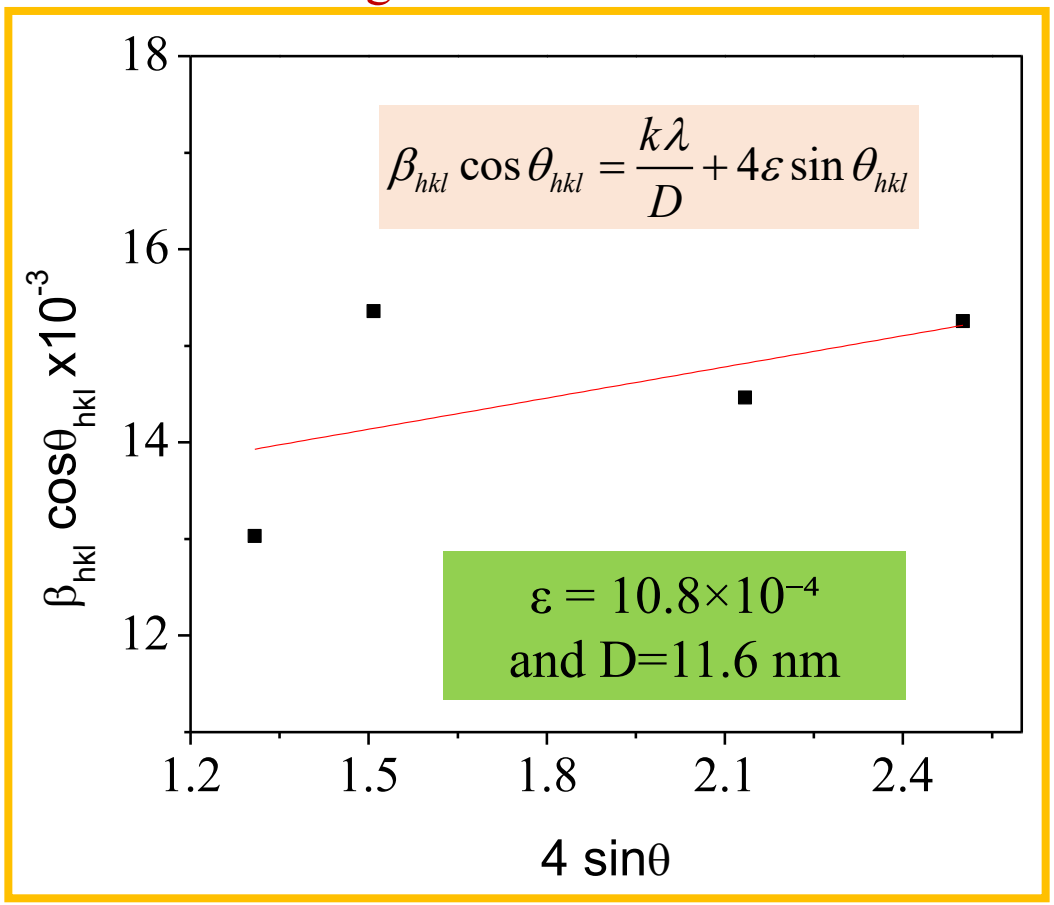
The average crystallite size obtained from the Scherrer analysis was approximately 10 nm.

Although the Scherrer method provides an approximate estimation of crystallite size, it attributes the observed sample-dependent peak broadening exclusively to finite crystallite dimensions and does not independently account for lattice microstrain.

The strain-induced contribution to diffraction-peak broadening can be expressed as:

$$\beta_{hkl} = 4\varepsilon.tan\theta$$

By combining the size- and strain-broadening contributions under the assumption of isotropic and uniform deformation, the Williamson–Hall method gives:



Crystallographic Directional Elastic Parameters

The conventional Williamson–Hall approach assumes isotropic strain. This approximation may not fully describe the actual deformation behaviour of a real crystalline material, particularly when the elastic response varies with crystallographic orientation. Therefore, hkl-dependent microstrain (ε_{hkl}) was evaluated by

$$\varepsilon_{hkl} = \left[\frac{d_{hkl} - d_{0(hkl)}}{d_{0(hkl)}}\right]$$

And $\varepsilon_{hkl}^{RMS} = \sqrt{\frac{2}{\pi}}(\varepsilon_{hkl})$

The corresponding effective directional stress was estimated using Hooke's law:

$$\sigma_{hkl} = \varepsilon_{hkl}^{RMS} Y_{hkl}$$

For a cubic crystal, the directional Young's modulus and Poisson's ratio can be calculated from

$$\frac{1}{Y_{hkl}} = S_{11} - 2\left(S_{11} - S_{12} - \frac{S_{44}}{2}\right)\left(\frac{h^2k^2 + k^2l^2 + l^2h^2}{(h^2 + k^2 + l^2)^2}\right)$$

$$\frac{1}{\upsilon_{hkl}} = -\frac{2S_{11} - 2\left(S_{11} - S_{12} - \frac{S_{44}}{2}\right)\left[1 - \frac{h^4 + k^4 + l^4}{(h^2 + k^2 + l^2)^2}\right]}{2S_{12} + \left(S_{11} - S_{12} - \frac{S_{44}}{2}\right)\left[\left(1 + \frac{h^4 + k^4}{(h^2 + k^2)^2}\right)\frac{l^2}{h^2 + k^2 + l^2} + \frac{2h^2k^2}{(h^2 + k^2)^2}\right]\frac{h^2 + k^2}{h^2 + k^2 + l^2}}$$

DFT-Based Evaluation of Directional Elastic Properties

The independent elastic compliance constants, S_{11}, S_{12}, and S_{44} were obtained from the corresponding elastic stiffness constants using the following expressions:

$$S_{11} = \frac{C_{11}+C_{12}}{(C_{11}-C_{12})(C_{11}+2C_{12})}; S_{12} = \frac{-C_{12}}{(C_{11}-C_{12})(C_{11}+2C_{12})}; S_{44} = \frac{1}{C_{44}}$$

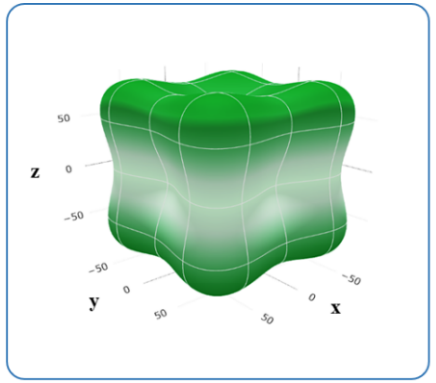
The DFT calculations yielded elastic stiffness constants of C_{11} = 135.9 GPa, C_{12} = 91.0 GPa, and C_{44} = 49.3 GPa, which satisfy the mechanical stability criteria for a cubic crystal, namely (C_{11}- C_{12}>0), (C_{11}+2C_{12}>0), and (C_{44}>0), confirming the mechanical stability of the calculated elastic tensor.

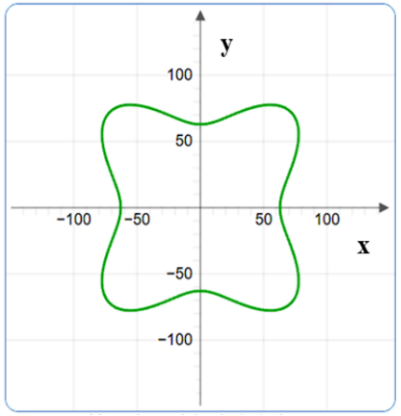
Using these stiffness constants, the corresponding compliance constants were calculated as S_{11} = 0.0159 GPa^{-1}, S_{12} = -0.0060 GPa^{-1}, and S_{44} = 0.0203 GPa^{-1}. These compliance constants were subsequently employed to evaluate the crystallographic-direction-dependent Young's modulus and Poisson's ratio.

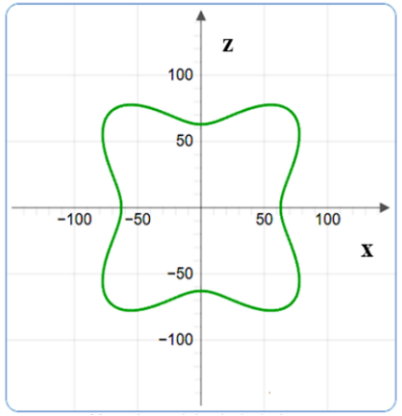
Plane	$\varepsilon_{hkl} \times 10^{-4}$	$\varepsilon^{RMS}_{hkl} \times 10^{-4}$	E_{hkl} (GPa)	υ_{hkl} (GPa)	σ_{hkl} (GPa)
(111)	12.72	10.15	128.0	0.299	0.130
(200)	4.89	3.90	62.9	0.401	0.025
(220)	6.92	5.52	101.7	0.340	0.056
(311)	8.12	6.48	82.7	0.408	0.054

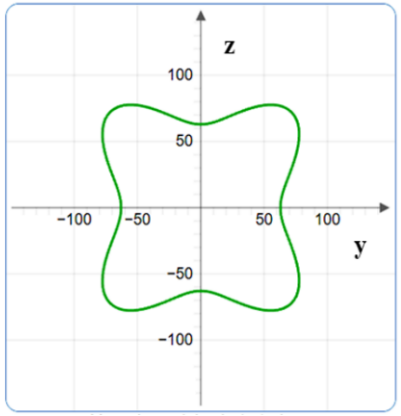
DFT-Based Evaluation of Directional Elastic Properties

For a more comprehensive visualization of this anisotropic elastic behaviour, the three-dimensional directional distribution of Young's modulus and Poisson's ratio and their corresponding two-dimensional projections along the xy, xz, and yz planes were generated from the DFT-derived elastic tensor.

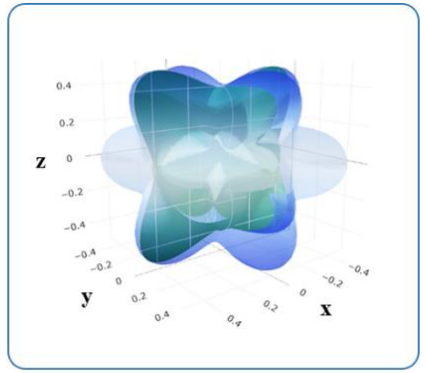


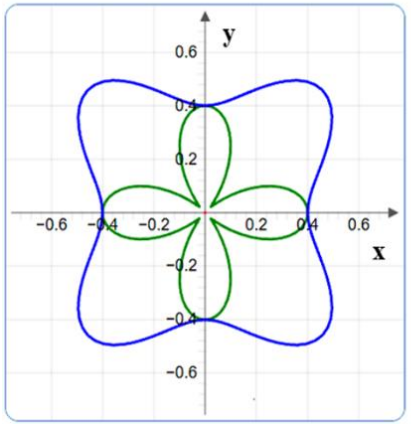


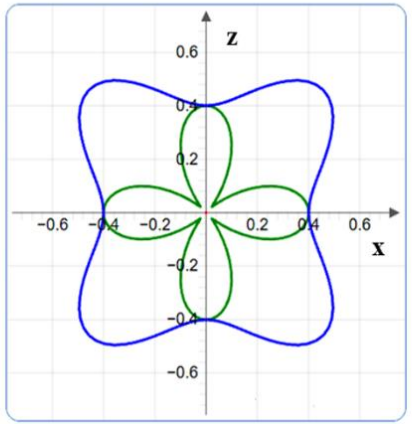


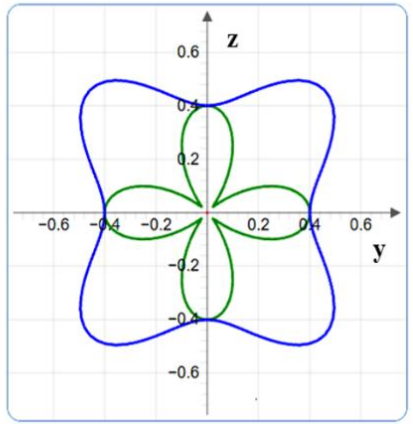


DFT-derived directional distribution of Young's modulus









DFT-derived directional distribution of Poisson's ratio

Conclusion

- The study establishes a useful relationship between the experimentally observed structural characteristics and the theoretically evaluated elastic response of nanocrystalline silver.
- XRD analysis provides information regarding the FCC crystal structure, lattice parameter, crystallite size, and crystallographic-direction-dependent lattice deformation.
- Using the experimentally obtained structural parameters, DFT calculations provide the intrinsic elastic stiffness and compliance constants necessary to evaluate directional mechanical properties.
- Integrating XRD and DFT enables a more comprehensive and accurate assessment of crystallographic-orientation-dependent elastic behavior than independent analysis.
- Combining experimental strain values with DFT-derived directional Young's modulus shows that the <111> direction exhibits the highest estimated effective stress due to its larger microstrain and higher directional Young's modulus.


Thank You